30.0 MICROSTRUCTURAL DEVELOPMENT OF METALLIC ALLOYS DURING RAPID SOLIDIFICATION

Chloe Johnson (Mines)
Faculty: Amy Clarke (Mines)
Other Participants: Yaofeng Guo (Mines), Jonah Klemm-Toole (Mines), Gus Becker (Mines), Francisco Coury (UFSCar), Joe Mckeown (Lawrence Livermore National Laboratory)
Industrial Mentor: Paul Wilson (Boeing) and John Carpenter (Los Alamos National Laboratory)

This project initiated in Fall 2017 and is supported by the George S. Ansell Department of Metallurgical and Materials Engineering Fellowship, A.J. Clarke's startup funds at the Colorado School of Mines (Mines), and CANFSA. The research performed during this project will serve as the basis for an Ph.D. thesis for Chloe Johnson.

30.1 Project Overview and Industrial Relevance

Understanding the relationship between processing, microstructure, and final performance of a metallic alloy is a fundamental goal of materials science. This begins with understanding the as-solidified microstructure, which can greatly impact subsequent solid-state microstructural evolution and final performance of a part. While conventional solidification techniques have been extensively studied, far from equilibrium processes that involve rapid solidification (e.g. additive manufacturing, AM) are not entirely understood. Processes like AM result in unique grain morphologies and metastable phases that can change the expected final properties of a metallic component. Because of this, it is important to understand the mechanisms controlling microstructural development during far from equilibrium processing to help predict and optimize performance.

Although rapid solidification studies have been performed on some aluminum alloys, most have involved post mortem characterization of microstructures. The advent of new in-situ techniques, with high spacial and temporal resolution, present an opportunity to peer into microstructural development during rapid solidification. While some studies have already been performed on a few binary aluminum alloys, many systems remain to be explored [30.1-30.3]. Few, if any, in-situ rapid solidification experiments have been performed on industrial aluminum alloys, and most ex-situ studies have focused on a limited selection of these alloys (mostly Al-Si alloys) [30.4]. This study proposes to use in-situ imaging techniques to understand microstructural development and correlate microstructural features to processing parameters during the rapid solidification of binary and industrial aluminum alloys. This will be coupled with ex-situ analyses to capture a range of solidification structures for different processing conditions. The alloys selected include Al-Ge, for investigation of metastable phase development, as well as 6061 and a 6061 reactive metal powder (RAM) alloy designed specifically for AM. This work will present the first in-situ solidification study performed on these RAM aluminum alloys. Investigating the effect of rapid solidification conditions on microstructural development in these alloys will help to inform alloy and parameter selection during processes like AM.

30.2 Previous Work

In-situ, rapid solidification studies have been performed on Al-Cu and Al-Si alloys using the Dynamic Transmission Electron Microscope (DTEM) at Lawrence Livermore National Laboratory (LLNL) [30.1]. This technique images the evolution of the melt-pool during rapid solidification, capturing the growth of microstructural features and allowing for the determination of solidification velocities as features develop. This technique has been used by our group to also image Al-Ge, mainly to further explore the development of the metastable monoclinic (M) phase and the metastable phase diagram proposed by Laoui and Kaufman, as shown in **Figure 30.1** [30.3]. The work of Laoui and Kaufman suggests that at compositions just below the solubility limit of the M phase (i.e. below 50.5 at. % Ge), the M phase is the primary phase, given sufficient undercooling. Above this limit, the stable β phase is the primary phase, and is typically surrounded by regions of α-phase dendrites, metastable M + α eutectic, or a combination of dendrites surrounded by stable or metastable eutectic. Previous work has focused on general characterization of the microstructures present in the melt pools, with recent development focusing on phase identification and local solute and solidification conditions driving the formation of observed microstructures.

In February 2019, in-situ solidification experiments were performed using the laser powder bed fusion (LPBF) AM simulator at the Advanced Photon Source (APS) at Argonne National Laboratory (ANL). These experiments allow for in-situ x-ray imaging of a laser raster or spot melt formed by selected parameters on plate, powder, or plate with powder samples. For samples containing powder, glassy carbon plates are appied to each side of the sample to contain the powder and set the powder layer thickness, based on the height of the base plate and the glassy carbon. The radiography data captured in these experiments allow for the extraction of solidification velocities, as well as observation of phenomena such as pore formation, powder interaction, etc. An image of this set-up, including example data, is shown in **Figure 30.2** [30.2]. 6061 and 6061 RAM alloys were chosen for these experiments to explore the effects of alloy composition and process parameters on grain morphology in these alloys. RAM alloys contain components that react to form innoculants to induce a higher nucleation rate, and therefore finer grains. This is important for processes such as AM, where many traditional industrial aluminum alloys have been found to produce columnar growth and hot tearing. The addition of nucleant particles/RAM powder has been found to reduce this effect in a few different alloy systems [30.5]. However, studies on the microstructural development of these alloys is fairly limited, especially in the realm of aluminum alloys. The goal of these experiments is to help fill the knowledge gap of microstructural development in newly developed RAM alloys with comparison to the well-understood industrial Al 6061 alloy, with special emphasis on the effect of alloy composition and processing parameters on transitions from columnar to equiaxed growth in these alloys. Recent work has focused on post mortem analysis of 6061 and 6061 RAM alloy samples, as well as image analysis of in-situ data.

30.3 Recent Progress

30.3.1 Post Mortem Analysis of Al 6061 & 6061 RAM Samples

Samples of 6061 wrought plate and 6061 RAM AM builds with a powder layer of either 6061 or 6061 RAM powder were generated through an initial round of experiments peformed with the AM simulator at the APS. These samples consisted of either singular spot melts or single rasters at various laser power and velocity settings. Initial imaging of the 6061 RAM powder is shown in **Figure 30.3**, which has a particle size ranging from 10-50 μm for the 6061 alloy powder (gray particles) and a range of 1-20 μm for the reactive powders (white and black particles). The 6061 alloy powder consists of the same gray particles, without the reactive powders. Post mortem analysis of these samples began with top down imaging of each melt pool, all of which were covered with an oxide layer (**Figure 30.4a & b)**. In some areas of the melt pool, however, this oxide layer was cracked or thin, allowing for the observation of the underlying grain structure, as shown in **Figure 30.4c & d**. The single spot melt of 6061 wrought shown in **Figure 30.4d** is representative of the columnar grains observed in most of these samples. Also shown in this image are solidification cracks, proposed to be from hot tearing, that were observed in most, if not all, of the 6061 wrought samples. Images taken from the in-situ data immediately after solidification of the final liquid also show what appears to be solidification cracking (**Figure 30.5**). The structure observed in the 6061 RAM alloy samples (**Figure 30.4c**) show equiaxed grains in this 2D field of view. However, cross sectioning of these melt pools will need to be performed to confirm if these grains are truly equiaxed or simply cross sections of elongated cells or dendrites. These grains appear to be much finer than even the smallest dimension of the columnar grains observed in the 6061 wrought alloys, and so far no cracking has been observed. These initial results are consistent with what was expected based upon the literature, but more work remains to be done to fully characterize microstructural development in these alloys, namely analysis of the cross-sections of these melt pools. The results from this initial round of experiments will serve to inform baseline parameters for the design of more specific experiments in the future, which may involve more complex laser programing (i.e. multiple rasters, time delay between rasters, etc.).

30.3.2 Image Analysis of In-situ Data for 6061 Based Alloys

Image processing of radiography data from in-situ studies peformed at the APS was done using ImageJ software. Using this software, the solidification velocity can be extracted from a series of images and correlated to specific details in the microstructure of each melt pool. Image processing can also be used to see different phenomena during solidification, such as possible cracking, porosity formation, powder interactions, etc. Some initial solidification velocity measurments are shown in **Figure 30.6** and summarized in **Table 30.1** below. These were taken from single rasters performed on 6061 wrought plate with 6061 RAM powder, 6061 RAM AM build plate with 6061 RAM powder, and 6061 wrought with 6061 powder all with laser settings of 416 W and 0.5 m/s. **Table 30.1** shows that

the solidification velocity in each sample oscillates around an average value of roughly 0.4-0.5 m/s, with the solidification velocity decreasing as more RAM 6061 alloy material is added to the sample. This is most likely due to the extra heat provided by the exothermic reaction of the reactive particles. It can also be noted that the different measured spots reveal different average solidification velocities. This is to be expected due to the melt pool shape, a slightly higher heat content at the edge of the melt pool where the laser was last experienced, as well as flow of the liquid in the melt pool. While few conclusions can be drawn from this data without more post-mortem analysis of the melt pool microstructures, these values provide proof of concept. These calculations will be used to correlate solidification conditions to specific details observed in the microstructure of the melt pools as post mortem analysis continues.

30.3.3 Phase Identification in Al-Ge DTEM Samples

Phase identification using electron diffraction revealed that M + α eutectic formation was observed in all Al-Ge alloy compositions, the richest being 76 at.% Ge. However, the morphology of these eutectics changed with composition (**Figure 30.7**), generally becoming more irregular with increasing Ge content. Regions containing α dendrites surrounded by α + β coupled growth were also observed in alloys of composition ranging from 60-63 at.% Ge. These regions were observed either near the edge of the melt pool, with a transition into a region of purely M + α eutectic, or were found to compromise the entire melt pool. For melt pools containing the former, the end of the dendrites in the transition region appear to be surrounded by a divorced M + α eutectic, instead of α + β coupled growth, which then transitions into an irregular M + α eutectic region (**Figure 30.7c**). It is proposed that the reason for this transition from dendritic and eutectic growth to simply eutectic has to do with the effect of the local volume fraction of primary β phase and its effect on local solute conditions, which in turn determines the solidification pathway. **Figure 30.8** gives an illustration of how this might occur. In areas of the melt pool with a higher volume fraction of β solidifiying from the melt initially, the remaining liquid is richer in Al than areas with a lower volume fraction of β. This liquid can become rich enough in Al to favor the formation of α phase dendrites, surrounded by either M + α or α + β eutectic. The formation of the latter between dendrites could be due to the more favorable formation of β at higher local Ge content, or the assistance of β particles in the nucleation of the β phase in this coupled growth region (**Figure 30.7f**). The transition to M + α eutectic at the end of the dendritic growth region might then be due to a slightly lower Ge content in the liquid, with the observation of a divorced eutectic, indicating a still relatively high Ge content to achieve a high volume fraction of the Ge-rich phase. It has also been found in other DTEM studies that solidification velocity increases towards the center of the melt pool, which would also favor formation of the M over the β phase [30.1]. The transition to different morphologies of M + α eutectic is most likely due to differences in local solute conditions, but further investigation is needed for a more detailed conclusion.

30.4 Plans for Next Reporting Period

- Post mortem investigation of grain morphology transitions in 6061 & 6061 RAM alloy melt pool cross sections and correlation to solidification velocities from image processing.
- Experimental planning for future, more complex experiments at the APS.
- Identification of mechanisms controlling morphological transitions in M + α eutectic in Al-Ge alloys.

30.5 References

[30.1] J. McKeown, A. Kulovits, C. Liu, K. Zweiacker, B. W. Reed, T. LaGrange, J.M.K. Wiezorek, G.H. Campbell, “In situ transmission electron microscopy of crystal growth-mode transitions during rapid solidification of a hypoeutectic Al-Cu alloy”, Acta Materialia, 2014, 65:56-68

[30.2] C. Zhao, K. Fezzaa, R. Cunningham, H. Wen, F. De Carlo, L. Chen, A.D. Rollett, T. Sun, “Real-time monitoring of laser powder bed fusion process using high-speed X-ray imaging and diffraction”, Scientific Reports, 2017, 7:3602

[30.3] T. Laoui and M. Kaufman, “Nonequilibrium behavior in the Al-Ge alloy system: insights into the metastable phase diagram”, Metallurgical and Materials Transactions A, 1991, 22(9):2141-2152

[30.4] A. I. Mertens, J. Delahaye, and J. Lecomte-Beckers, “Fusion-based additive manufacturing for processing aluminum alloys: state-of-the-art and challenges”, Advanced Materials Engineering, 2017, 19(8):1-13

[30.5] J. H. Martin, B. D. Yahata, J. M. Hundley, J. A. Mayer, T. A. Schaedler, T. M. Pollock, “3-D printing of high-strength aluminium alloys”, Nature, 2017, 549 303-314

30.6 Figures and Tables

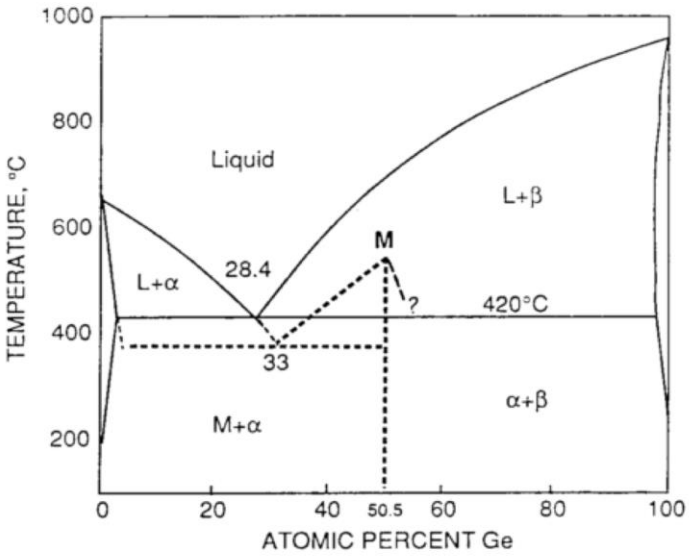

Figure 30.1: Al-Ge phase diagram, showing the proposed metastable phase diagram for the metastable monoclinic (M) phase [30.4].

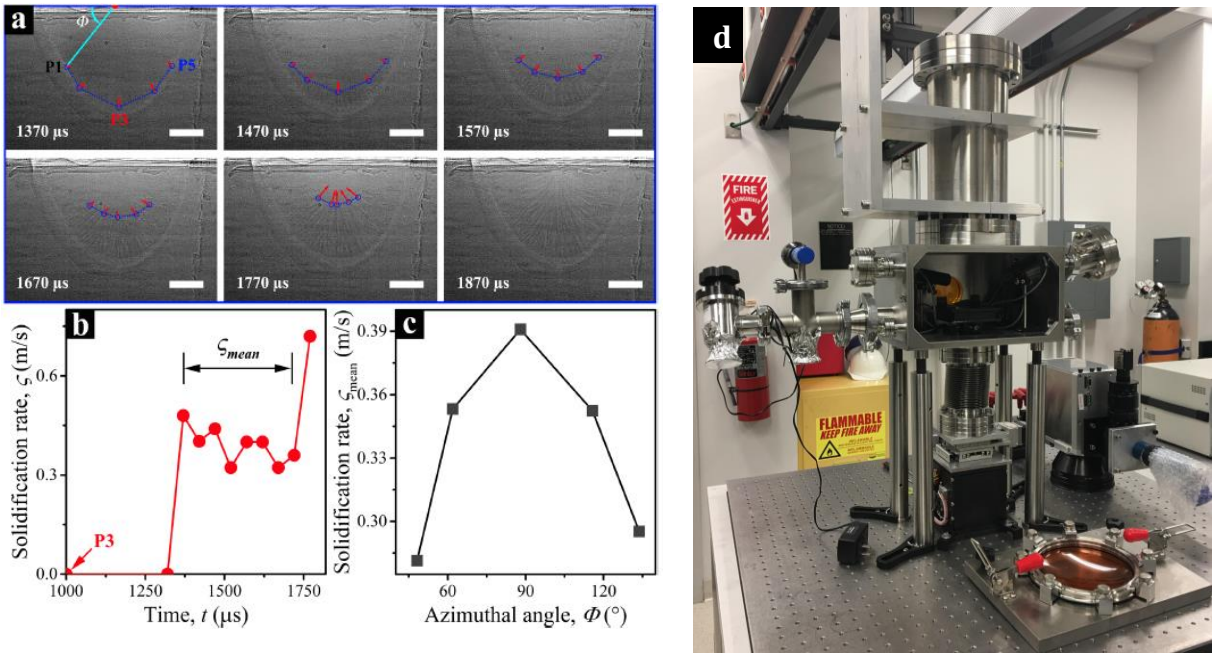

Figure 30.2: a) Example imaging of spot melts from radiograpy experiments performed on Ti-6-4 using the AM simulator at the APS. b) & c) solidification velocity data and azimuthal angle exracted from the images shown in a); red arrows show where these points were taken. d) An image of set up at the APS. The center box shows where the sample is contained under vacuum; the laser beam hits the sample from above, traveling through the vertical column, while an x-ray beam is transmitted through the sample into the picture [30.3].

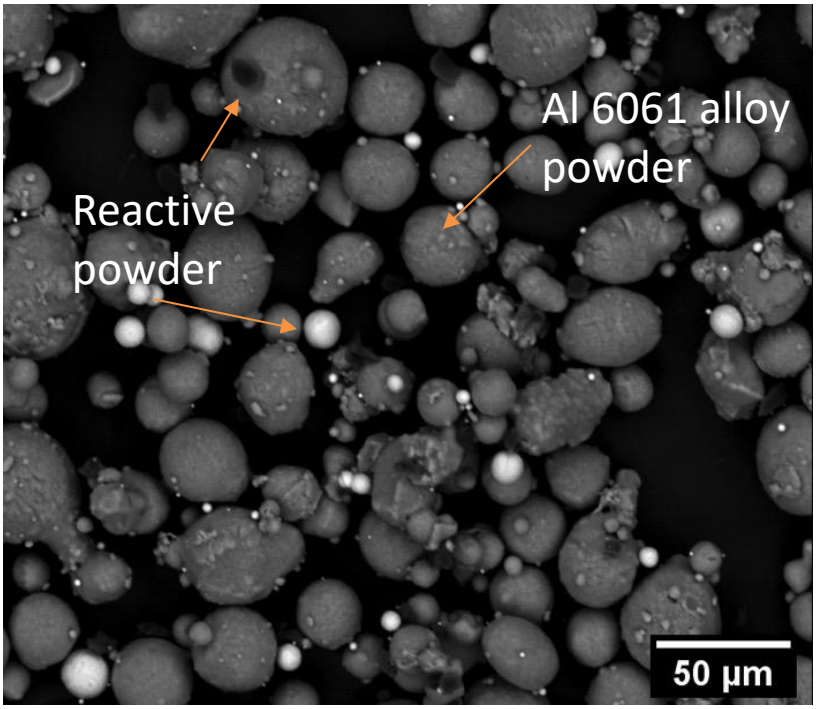

Figure 30.3: A BSE SEM image of Al 6061 RAM alloy powder. The white and black particles show the smaller RAM powder, while the larger gray particles are the 6061 alloy powder. The baseline 6061 alloy powder used in these studies was the same powder as the gray particles shown in this image.

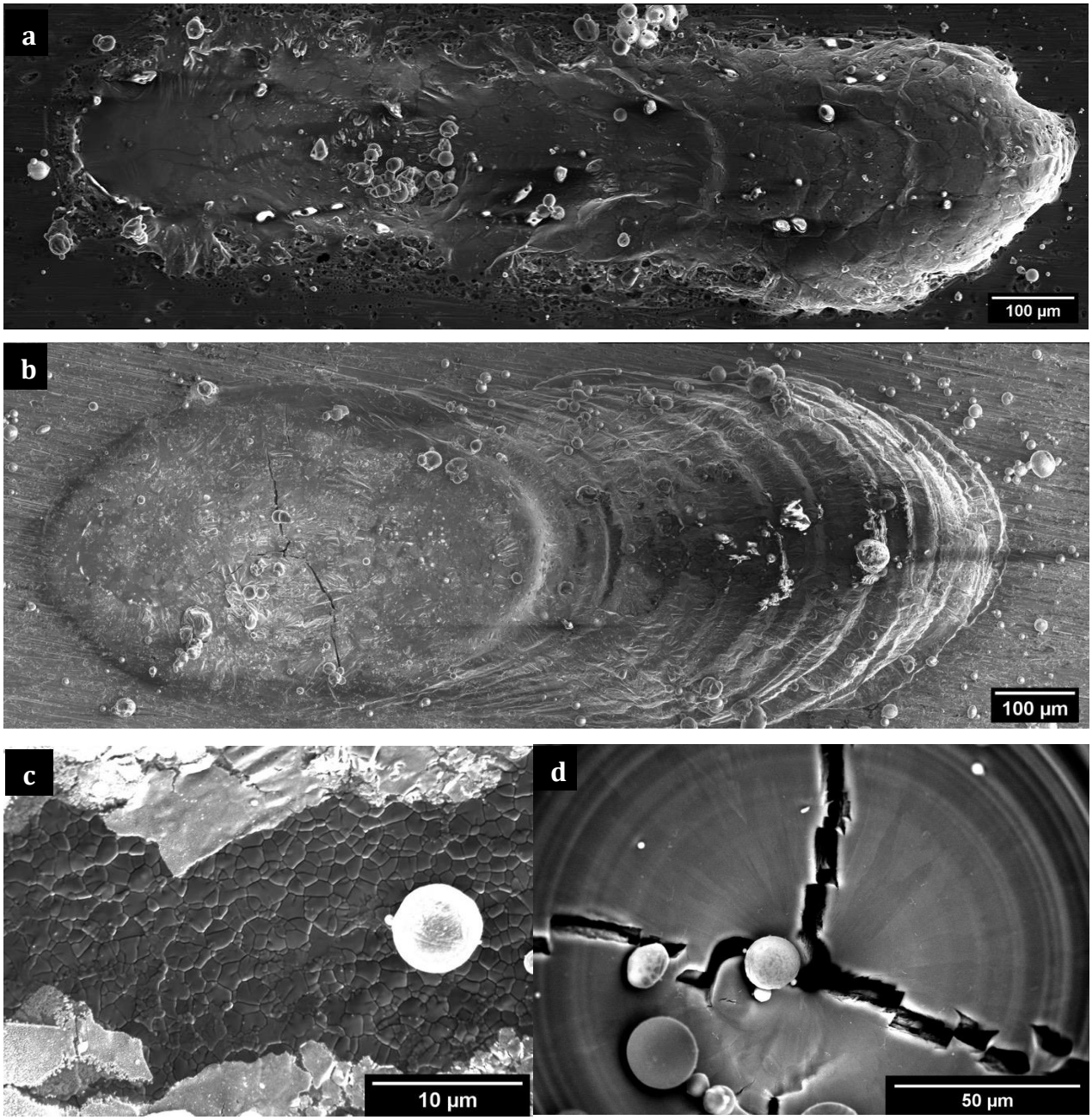

Figure 30.4: a) Secondary electron SEM image of a laser raster of an Al 6061 RAM AM build base plate with Al 6061 RAM powder on top with laser settings of 416 W and 0.3 m/s. b) Secondary electron SEM image of a laser raster with the same settings done on a 6061 wrought base plate with 6061 powder on top. c) Higher magnification image of the grain structure in raster a), taken from an area where the oxide layer has been cracked/removed. d) A BSE SEM image of a spot melt of 6061 wrought base with 6061 powder at 520 W and 2 ms showing evidence of columnar grains and hot tearing.

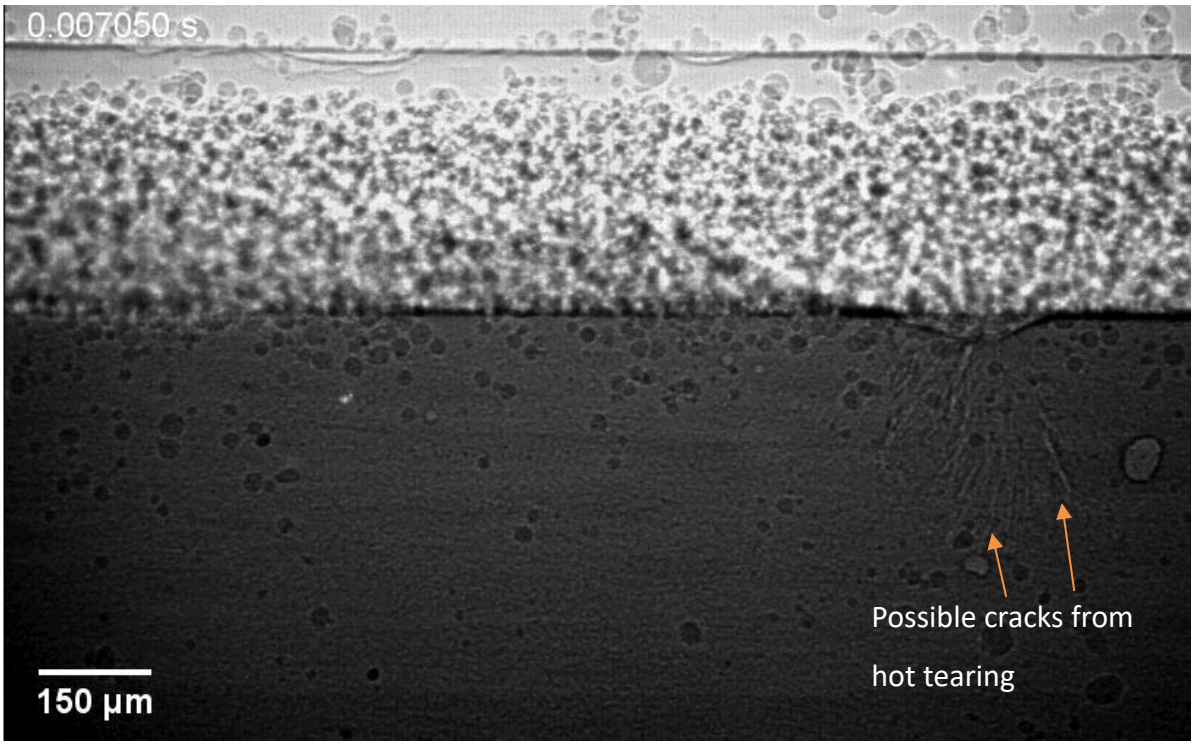

Figure 30.5: Image taken from radiography data of a 6061 wrought base plate with 6061 powder (laser power 512 W, speed of 0.3 m/s), showing possible hot tearing after solidification of melt.

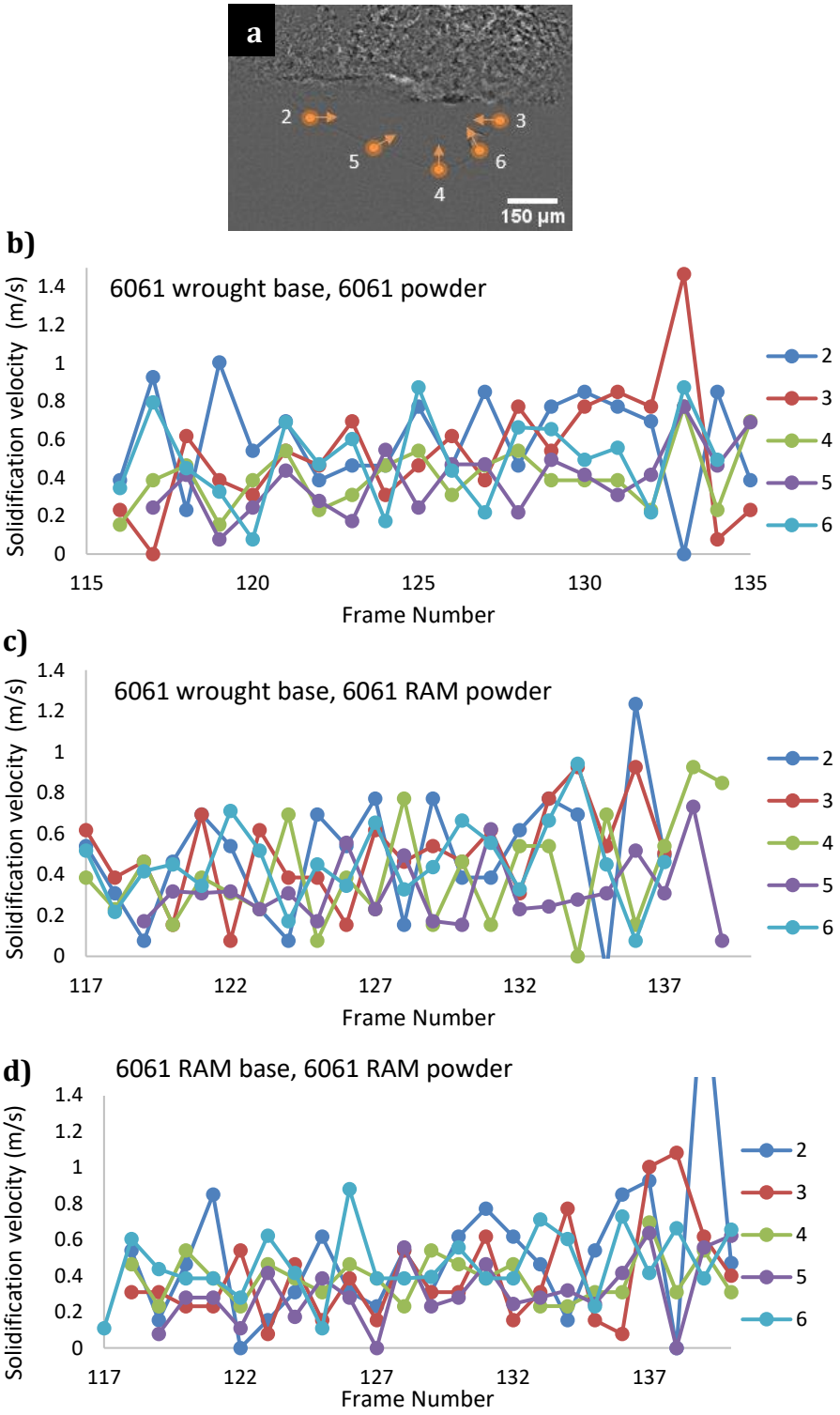

Figure 30.6: a) Location of measurement points 2-6. b), c), & d) solidification velocity calculations for 6061 wrought base with 6061 powder, 6061 wrought base with 6061 RAM powder, and 6061 RAM base with 6061 RAM powder all at a laser power of 412 W and speed of 0.5 m/s.

Table 30.1: Average velocity and standard deviation values for each point in each material						
	6061 wrought, 6061 Powder		6061 wrought, 6061 RAM		6061 RAM, 6061 RAM	
Point	Average Velocity (m/s)	Standard Deviation	Average Velocity (m/s)	Standard Deviation	Average Velocity (m/s)	Standard Deviation
2	0.60	0.2589	0.49	0.3112	0.47	0.2638
3	0.52	0.3252	0.51	0.2329	0.40	0.2805
4	0.40	0.1654	0.41	0.2573	0.39	0.1226
5	0.39	0.1750	0.32	0.1688	0.32	0.1895
6	0.50	0.2324	0.46	0.2033	0.48	0.2097

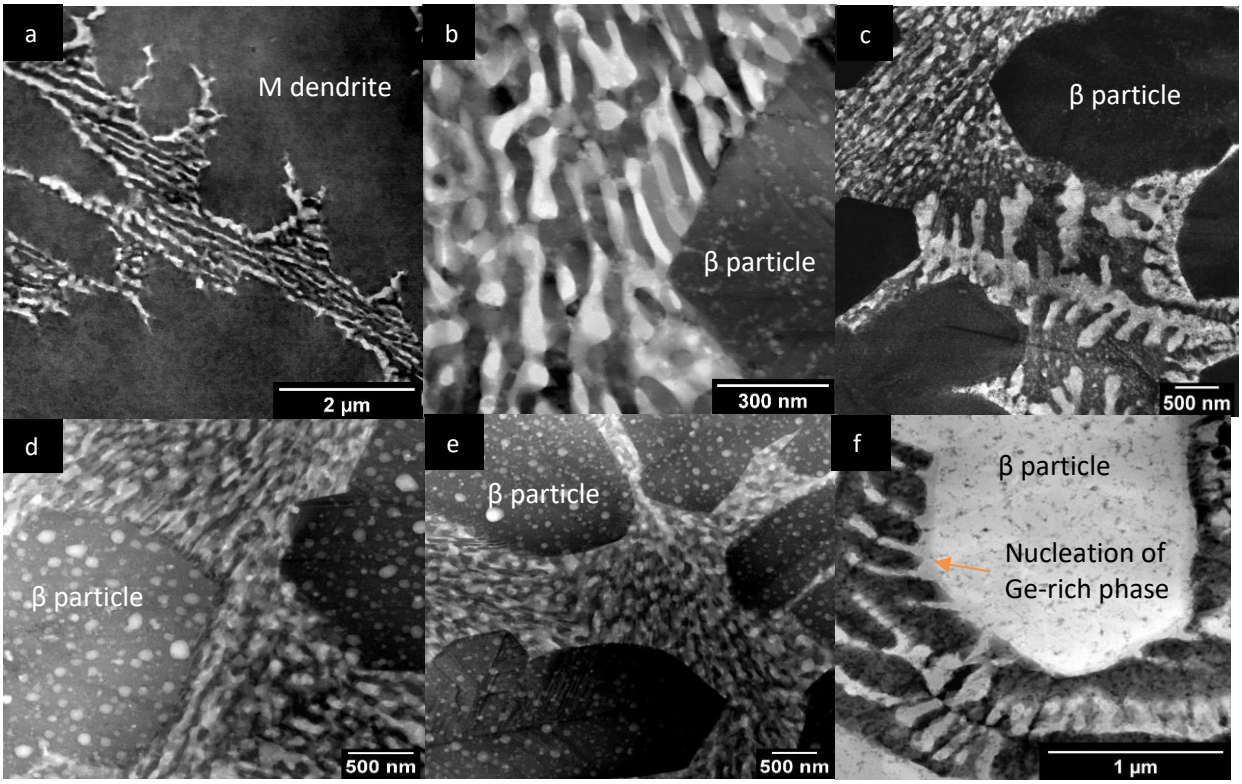

Figure 30.7: Bright field STEM images of various observed morphologies of M + α eutectic in different Al-Ge alloys, with compositions of a) 46, b) 58, c) 60-63, d) 63-69, and e) 70-76 at.% Ge. The darker phases are Ge rich, while the ligher phases are Al rich. It can be seen as the Ge content of the sample increases, the morphology of the eutectic appears to become more irregular. The 60-63 at.% Ge alloy in c) shows two different morphologies, namely that surrounding the α phase dendrite, which appears to be a divorced eutectic, and that further away from the dendrite. f) Is a HAADF STEM image showing the nucleation of a Ge rich (now light colored) phase nucleating off of a β phase particle to grow between dark, α phase dendrites in a 63 at.% Ge sample. Images taken by Yaofeng Guo and Francisco Coury.

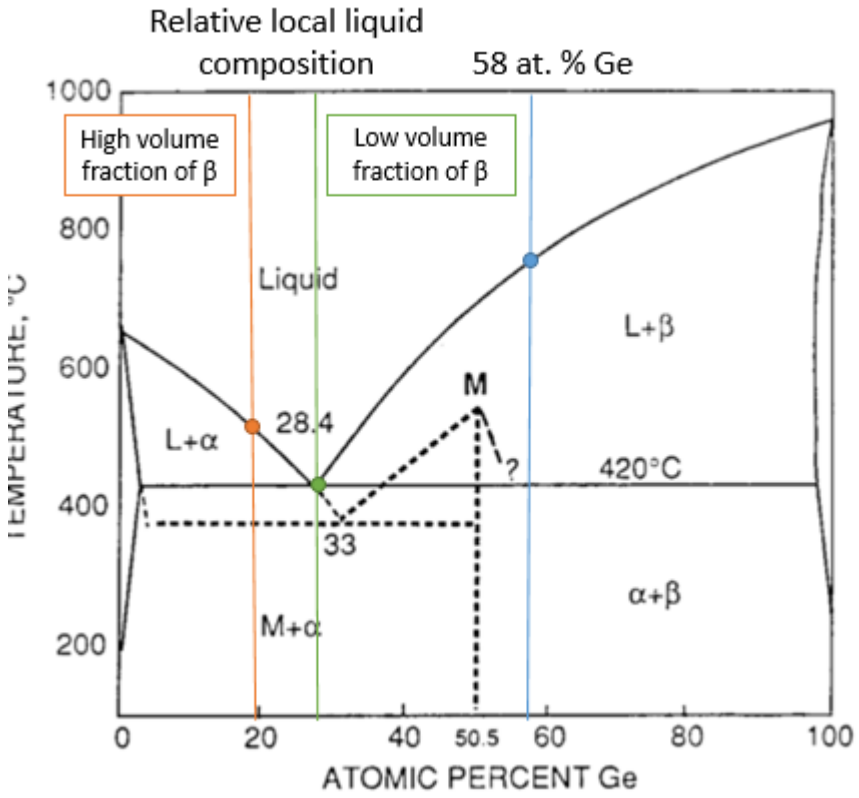

Figure 30.8: Al-Ge phase diagram, showing the proposed metastable phase diagram for the metastable monoclinic (M) phase [30.4], as well as possible solidification pathways for an area of the melt pool with a relatively high (orange line) versus a relatively low (green line) volume fraction of β for an example alloy of 58 at.% Ge (blue line).